Pulsed Plasma Thruster Plume Study: Symmetry and Impact on Spacecraft Surfaces

Lynn A. Arrington
Dynacs Engineering Company, Inc., Brook Park, Ohio

Colleen M. Marrese and John J. Blandino
Jet Propulsion Laboratory, Pasadena, California

September 2000

The NASA STI Program Office . . . in Profile

Since its founding, NASA has been dedicated to the advancement of aeronautics and space science. The NASA Scientific and Technical Information (STI) Program Office plays a key part in helping NASA maintain this important role.

The NASA STI Program Office is operated by Langley Research Center, the Lead Center for NASA's scientific and technical information. The NASA STI Program Office provides access to the NASA STI Database, the largest collection of aeronautical and space science STI in the world. The Program Office is also NASA's institutional mechanism for disseminating the results of its research and development activities. These results are published by NASA in the NASA STI Report Series, which includes the following report types:

- TECHNICAL PUBLICATION. Reports of completed research or a major significant phase of research that present the results of NASA programs and include extensive data or theoretical analysis. Includes compilations of significant scientific and technical data and information deemed to be of continuing reference value. NASA's counterpart of peer-reviewed formal professional papers but has less stringent limitations on manuscript length and extent of graphic presentations.

- TECHNICAL MEMORANDUM. Scientific and technical findings that are preliminary or of specialized interest, e.g., quick release reports, working papers, and bibliographies that contain minimal annotation. Does not contain extensive analysis.

- CONTRACTOR REPORT. Scientific and technical findings by NASA-sponsored contractors and grantees.

- CONFERENCE PUBLICATION. Collected papers from scientific and technical conferences, symposia, seminars, or other meetings sponsored or cosponsored by NASA.

- SPECIAL PUBLICATION. Scientific, technical, or historical information from NASA programs, projects, and missions, often concerned with subjects having substantial public interest.

- TECHNICAL TRANSLATION. English-language translations of foreign scientific and technical material pertinent to NASA's mission.

Specialized services that complement the STI Program Office's diverse offerings include creating custom thesauri, building customized data bases, organizing and publishing research results . . . even providing videos.

For more information about the NASA STI Program Office, see the following:

- Access the NASA STI Program Home Page at *http://www.sti.nasa.gov*

- E-mail your question via the Internet to help@sti.nasa.gov

- Fax your question to the NASA Access Help Desk at (301) 621-0134

- Telephone the NASA Access Help Desk at (301) 621-0390

- Write to:
  NASA Access Help Desk
  NASA Center for AeroSpace Information
  7121 Standard Drive
  Hanover, MD 21076

Pulsed Plasma Thruster Plume Study: Symmetry and Impact on Spacecraft Surfaces

Lynn A. Arrington
Dynacs Engineering Company, Inc., Brook Park, Ohio

Colleen M. Marrese and John J. Blandino
Jet Propulsion Laboratory, Pasadena, California

National Aeronautics and
Space Administration

Glenn Research Center

September 2000

Acknowledgments

PULSED PLASMA THRUSTER PLUME STUDY:
SYMMETRY AND IMPACT ON SPACECRAFT SURFACES

Lynn A. Arrington
Dynacs Engineering Company, Inc.
Brook Park, Ohio 44142

Colleen M. Marrese and John J. Blandino
Jet Propulsion Laboratory
California Institute of Technology
Pasadena, California 91109

Abstract

Twenty-four witness plates were positioned on perpendicular arrays near a breadboard Pulsed Plasma Thruster (PPT) to collect plume constituents for analysis. Over one million shots were fired during the experiment at 43 J using fluorocarbon polymer propellant. The asymmetry of the film deposition on the witness plates was investigated with mass and thickness measurements and correlated with off-axis thrust vector measurements. The composition of the films was determined. The transmittance and reflectance of the films were measured and the absorption coefficients were calculated in the wavelength range from 350 to 1200 nm. These data were applied to calculate the loss in signal intensity through the films, which will impact the visibility of spaceborne interferometer systems positioned by these thrusters.

Introduction

Pulsed plasma thrusters (PPTs) are low thrust electric propulsive devices which have a low power requirement, less than 120 Watts, and high specific impulse greater than 1200 seconds.[1] PPTs can provide spacecraft attitude adjustments, high-precision positioning, and orbit raising on small satellite missions. Because of their high specific impulse and small minimum impulse bit capabilities, PPTs, have recently been considered for spaceborne interferometers on Space Technology 3 (ST-3) and Terrestrial Planet Finder (TPF), which require precise position maintenance.

Concerns have been raised about plume induced spacecraft contamination, which can affect performance of the solar arrays and on-board instruments. Data from the NOVA spacecraft have shown no conclusive evidence of solar array degradation when PPTs were fired in close proximity to the arrays.[2,3] The optical interferometer which will be used on ST-3 has siderostats and transfer flats which reflect two starlight signals towards a beam combiner. These elements of the system will be exposed to the space environment and could be subject to contamination. Films, which condense on these surfaces, could affect signal intensities and wavefronts resulting in a reduction in performance of the interferometer instrument. One parameter used to quantify instrument performance is the visibility, which is discussed in detail in a later section. The optical properties of these films must to be understood to assess their impact on instrument visibility.

Recently a breadboard (BB) PPT was tested and samples of thruster effluents collected. This was done to investigate the symmetry of the PPT plume and study the physical and optical properties of the films formed when the effluents condense on a witness plate. This study further addresses concerns about the optical properties of the films deposited by the thruster that were raised in a previous study,[4] conducted at Glenn Research Center, with the same BB PPT. The results of the previous study showed that in the plane parallel to the electrode pairs, the symmetric case, the off-axis thrust component was below the detection threshold of the thrust stand. However in the asymmetric plane of the PPT, the plume was canted towards the cathode electrode resulting in a thrust vector towards the anode electrode. It was suspected that the plume was not symmetric around the PPT primary thrust axis. The present, more extensive study was conducted as a follow up to a previous study[5] where only partial far-field planes of a PPT were examined. The objective of the research presented in this article was to determine the symmetry/asymmetry of a PPT plume by characterizing the films deposited on local witness plates. The films collected from the thruster discharge were characterized to determine their composition, thickness, transmittance,

and reflectance. This information was used to correlate the off-axis thrust vector and its potential impact on spacecraft instrument visibility. The results of this test can be applied to help predict and control the contamination deposition rates on sensitive spacecraft surfaces with the orientation of the PPT.

This paper discusses the configuration of the PPT with a description of the test set-up in the vacuum facility. Included is a discussion of the measurements conducted on samples both prior to and following exposure to the PPT plume. Instrument visibility is explained and data acquired from these tests are used to assess the impacts of PPT effluents on surrounding instrumentation in future spacecraft missions.

Test Description

The contamination experiment was conducted in a high vacuum facility using a breadboard PPT. For this experiment, quartz slides were used as witness plates. Witness plates were mounted on two contamination rakes that were placed downstream of the PPT. Data were not taken for the back flow region behind the exit plane of the PPT. Prior to testing, the surface of each plate was cleaned with ethanol and dried. The plates were exposed to a plume produced by the PPT operating at a single discharge energy level for over a million pulses. Pre- and post-test measurements collected from the witness plates included reflectance, transmittance, mass, thickness, and composition.

Experimental Apparatus

Contamination Rake

Two mutually perpendicular semicircular arrays were placed in the plume. There were a total of 24 samples including three control samples. Collimators were positioned every 20° through 180° on the arrays, as shown in Figure 1. Quartz witness plates were positioned at the back of each collimator. Each collimator was aligned so that the center axis of the collimator would intersect the geometric centerline of the fuel bar face at the PPT exit plane. Each array included horizontal collimators at positions #1, 11, 12, and 21 as shown in Figure 1. An additional collimator was placed at the intersection of the arrays, the 90° position (sample #6), facing directly into the PPT. The array with samples #1 through #11 was located in a plane that was perpendicular to the faces of the electrode pairs. Sample #1 was located closer to the anode electrode, while sample #11 was closer to the cathode electrode, making it the

asymmetric array. The array with samples #12 to #21 was positioned parallel to the electrode faces, in the symmetric array. The radius of each array was 61 cm.

A schematic of a collimator is shown in Figure 2. The collimator was lined with tantalum foil and had two tantalum apertures to restrict the field of view of quartz slide. Each quartz slide was held between two sheets of molybdenum. One sheet had a 2.5 cm diameter hole in it. This device held the 2 cm x 2 cm square quartz slide only at its corners. Tantalum and molybdenum were used to reduce sputtering and because these metals are not found elsewhere in the tank. The RMS surface roughness of the quartz slides before exposure to the PPT plume was <50Å.

Diagnostics

A double beam, double-monochromator, ratio recording spectrometer, operating in the ultraviolet, visual and near infrared spectral ranges, was used to make optical measurements on the samples. Reflectance and transmittance measurements were taken over a range of wavelengths from 350 nm to 1200 nm. The direct measurements were made over a 1.0 cm x 1.8 cm area of each slide. An integrating sphere within the spectrometer determines the sum of the specular and diffuse light to give total reflectance. An oddity in the manufacture of this particular spectrometer has caused an uncertainty of specular measurements to be approximately 10%. However, the measurements made here were primarily diffuse in nature and the uncertainty is less than a few percent and relative to each other the measurements should be even accurate since they were made one right after the other. The resolution of the instrument was set to 1 nm. The smoothing interval of the instrument was set too low for data averaging (curve smoothing) across the wavelength scan to occur.

The film thickness and surface composition were determined by Auger Electron Spectroscopy (AES) for samples with a net deposition. Each sample was installed in the spectrometer at base pressure of approximately 10^{-9} torr, then the chamber was backfilled with argon to a pressure of approximately 10^{-5} torr. The sample surface was sputtered using an ion gun operating at 1 to 2 kV and a 5 kV electron beam rastered over an area of 0.01 mm^2 was used for analysis. A cylindrical mirror analyzer was used to collect data. During sputtering the composition of the film material was monitored, and through a calibration process the thickness of the films was determined.

Profilometer measurements were taken to determine etch depths where net ablation occurred. The profilometer measurements were made near the interface of the exposed and non-exposed surfaces of the witness plates. The profilometer used had a probe radius of 5 microns.

Pulsed Plasma Thruster

The thruster used in this study, shown in Figure 3, was a breadboard PPT built by Primex Aerospace under a contract with Glenn Research Center.[5] It is a rectangular PPT, where the fluorocarbon polymer propellant is fed between parallel electrodes. A high voltage capacitor, connected across the electrode pair, is discharged by a single spark plug across the face of the propellant. The charge-up time of the capacitor is generally on the order of hundreds of milliseconds, while the discharge occurs on the order of tens of microseconds. The high energy discharge in turn ablates the propellant surface, ionizes it, and accelerates it away from the surface providing thrust. The constituents of this plume are carbon, fluorine, and a variety of fluorocarbons including CF_3, CF_2, and CF. Previous studies have shown the plume consists of both accelerated particles and slow neutrals.[6, 7]

The BB PPT was pulsed approximately 1.25 million times at a frequency of 1 Hz and an energy level of 43 Joules. Though the testing was interrupted from time to time, the tank remained at vacuum from start to finish. The performance measured for this PPT in a previous study[3] was shown to have an average impulse bit of 710 μN-sec, with an average mass loss of 60.3 μg/pulse.

Test Facility

The vacuum facility used for this test is at the NASA Glenn Research Center. The tank is 1.52 m in diameter and 3.05 m high with a 0.51 m cryopump. The facility base pressure is generally in the mid 10^{-7} torr range and the pressure during the experiments was in the mid 10^{-6} range. The PPT main capacitor and power processing unit (PPU) were mounted to a copper cooling plate maintained at about 20° C, to prevent capacitor overheating during the long duration run. The PPT was hung at top of the tank, with the nozzle pointing down along the chamber centerline. The witness plates were positioned below the thruster so that horizontal collimators were aligned with the exit plane of the PPT. The films collected represent a worst case scenario of the film deposition rate on the witness plates due to facility effects including backsputtered facility materials. To reduce facility effects, the collimators are designed with a limited field of view and fabricated from low sputter yield materials. Also, baffles located in the bottom of the tank to trap some of the material sputtered off of the tank wall.

Impact on Interferometer Visibility

The visibility parameter is an important figure-of-merit to quantify performance of the proposed spaceborne interferometers. A number of effects will degrade the visibility from an ideal value of one. A strict instrument visibility budget places severe constraints on spacecraft contamination by the thruster effluents. Total visibility, Γ_{Total}, depends on both source, Γ_*, and instrument, $\Gamma_{Instrument}$, visibility($\Gamma_{Total}=\Gamma_*\Gamma_{Instrument}$). Instrument visibility must be known to quantify instrument performance, isolate source visibility for science missions, and determine the time period required for observations. It is also important to understand its time variability to determine the frequency of calibrator source observations required. Material discharged from the thruster can be deposited on the interferometer instrument to reduce visibility by decreasing transmissivity (to decrease signal intensity), increasing reflectivity (which results in an increase in background noise after interactions with the spacecraft), and causing wavefront phase distortions in the spectral range of interest (which reduces the visibility of the interference fringes). The spectral range of interest for ST-3 is 450-1000 nm, and the spectral range of interest for TPF will be approximately 1-15 μm. ST-3 will fly a collector spacecraft with a siderostat and transfer flat, and a combiner spacecraft with two siderostats which could be affected by the thruster effluents.[8] The source signals will pass through the surfaces of each of these elements twice before interacting with the next element. The cumulative effects of each surface must be considered in determining the instrument visibility. Mission requirements for ST-3 include maintaining a broadband (620-1000 nm)[9] instrument visibility during fringe searching which is greater than 0.42 and a narrowband (450-1000 nm)[9] visibility during fringe measurements which is greater than 0.42.[9] Considering the ST-3 instrument configuration and materials, broadband $\Gamma_{Instrument}$ is ~0.53 with a margin of 0.8, for a visibility budget of 0.42. The margin was introduced to account for error in the visibility factors in $\Gamma_{Instrument}$.

The total instrument visibility is determined by the following equation:

$$\Gamma_{Instrument}=\Gamma_{Phasing}\Gamma_{Pointing}\Gamma_{Dispersion}\Gamma_{Wavefront}\Gamma_{Intensity}\Gamma_{Area}$$

The thruster effluents will not affect all of these terms. Only $\Gamma_{Intensity}$ is addressed in this study. $\Gamma_{Phasing}$ and $\Gamma_{Pointing}$ are primarily time dependant effects with time scales less than the time allocated for each observation.

The thruster could affect the remaining terms over much longer time scales, remaining constant during each observation. $\Gamma_{Phasing}$ is affected when the two source signals are not in phase with each other because of different path lengths. The delay line in the combiner spacecraft increases the path length of one signal to equal the second, however it can not compensate for mechanical vibration in the instrument. This term is estimated to be 0.99 for ST-3.[9] $\Gamma_{Pointing}$ is affected when the signal is not properly directed to each of the interferometer elements and the area of the source signal is reduced because not all of the signal is intercepted. This term is reduced by alignment errors in the interferometer system, and is assumed to be 0.96 for ST-3.[9]

$\Gamma_{Dispersion}$ is reduced when a frequency dependent phase shift is introduced in the signal from interactions with the instrument before reaching the combiner. This value is estimated at 0.9 for broadband fringe searching and 0.97 for narrowband fringe measurements for the interferometer on ST-3.[9] The thruster effluents deposited as films could cause a reduction in this visibility term. The index of refraction as a function of wavelength must be measured for the specific films expected to evaluate $\Gamma_{Dispersion}$.

Interactions with a PPT will have the greatest impact on the $\Gamma_{Wavefront}$, where $\Gamma_{Wavefront}$ decreases with increasing variance of the average phase of the wavefront. The wavefront distortions are caused by non-uniform film thickness with dimensions on the order of and larger than the observing wavelengths. With a RMS film thickness t_{RMS} and signal wavelength λ,

$$\Gamma_{Wavefront} = e^{-\frac{\left(\frac{t_{RMS}}{\lambda}2\pi\right)^2}{2}}.$$

As an example, for a t_{RMS} of only 26 nm results in a $\Gamma_{Wavefront}$ of 0.93 for a 630 nm wavelength after passing through that surface twice (as will be the case with the siderostats and transfer flats). If the PPT effluents reduce the visibility within the margin of 0.8 (available for ST-3), and each of the four surfaces is affected similarly by the thruster, the tolerable RMS film thickness on each of the four surfaces can be 23.7 nm. Larger t_{RMS} will decrease the instrument visibility to below 0.47, and the required observation times will have to increase beyond the current objectives. In an early mission study, it was estimated that a siderostat could collect a ~6 nm fluorocarbon film during the ST-3 mission.[8] A non-uniform deposition of this film over

interferometer instrument elements should reduce the visibility within the tolerable margin, however, t_{RMS}, must be quantified for the specific films expected to determine $\Gamma_{Wavefront}$. This factor is currently estimated to be 0.625 for the ST-3 interferometer, accounting for all of the elements in the system, but could be further reduced by the PPT effluents.[9]

Interactions with the surfaces in the instrument will also reduce the intensity of the source signals before reaching the combiner. A difference in the intensity of each of the signals will reduce the visibility of the fringes in the interference pattern generated by the combined signals. The visibility of a fringe can be expressed in terms of the maximum and minimum intensity on the fringe pattern, and in terms of the electric field strengths, E, in the two beams before combination.[9]

$$\Gamma_{Intensity} = \frac{I_{Max} - I_{Min}}{I_{Max} + I_{Min}} = \frac{(E_1 + E_2)^2 - (E_1 - E_2)^2}{(E_1 + E_2)^2 + (E_1 - E_2)^2} = \frac{2(E_2/E_1)}{1 + E_2^2/E_1^2} = \frac{2\sqrt{K}}{1 + K},$$

where K is the ratio of intensities in the two beams before combination, which can be defined by T_1/T_2. The signal intensities will decrease with increasing film absorptance and transmittance, which are frequency dependent. A mismatch in the intensities of two signals of 40% (T_1=60 %, T_2=100 %) corresponds to a $\Gamma_{Intensity}$ of 0.968. $\Gamma_{Intensity}$ is assumed to be 0.986 for the interferometer on ST-3.[9] The films deposited by the thruster could further reduce this term. The transmittance losses through the specific films expected must be quantified to evaluate $\Gamma_{Intensity}$.

Particulates on the elements in the interferometer will reduce the area of the signal collected and Γ_{Area}. Carbon flakes from the PPT electrodes or propellant rod and fluorocarbon particulates can affect this visibility term. The most adverse effect will be caused by totally reflecting or absorbing particles. Γ_{Area} is defined by the ratio of the total area of the particulates or flakes to the area of the signal. The siderostats diameter on ST-3 will be 12 cm. The active area for signal collection will be 144 cm^2, therefore, particulates on the surfaces of the various elements in the interferometer would have to block 1.44 cm^2 of the signal to reduce Γ_{Area} to a value of 0.99. The size and density distribution of particulates and flakes deposited by thruster must be determined to evaluate Γ_{Area}.

Results and Discussion

Film characterization
Changes in the masses of the witness plates are shown in Table 1. A typical pre-test slide mass was in the range of 0.68-0.72 g, with an uncertainty of +/-0.046mg. The mass changes in control samples #22-24 were less than the

uncertainty, as expected, and showed that exposure to atmospheric conditions during the pre-test and post-test measurements did not impact the results. Samples #5-8 and #15-18 experienced a measurable mass loss with the exception of sample #9. Large changes were expected on these particular samples because they were located with the main body of the plume. These plates had been etched and had a frosty white appearance. Remaining samples all showed mass gain, but amount of change was a much smaller percentage of the total slide mass, which is expected as the sample positions move away from the mechanical centerline of the PPT. The plates that were located at 30 $^{\circ}$ and 50° from the vertical axis provided the most insightful measurements in determining the symmetry of the plume. Film thicknesses were also required to determine plume symmetry. Auger Electron Spectrometer (AES) measurements were initially intended to be performed on all the plates; however, the roughened non-conductive surfaces induced severe charging on plates #5-#8 and #15-#18. Therefore a different approach was required. Profilometer measurements were made at the interface of the exposed and non-exposed on the plates. The measurements show a significant difference in surface roughness between the exposed area, which was ablated, and the shielded area. An example of a profilometer measurement is shown in Figure 4. Because of the non-uniform ablation, an average depth was determined. The data collected on the samples mentioned above are given in Table 1. The profilometer range of motion, parallel to the surface of the plate was only a few mm, therefore variations across the exposed area of the plates could not be evaluated.

AES measurements of film composition and etch depth profiles were performed on the remaining 17 samples. In most cases, the surface was composed of fluorocarbons. An example of a surface scan is shown in Figure 5. The electron and ion beams that are used for the AES depth profiling analysis desorb fluorine. The actual fluorine level is then expected to be much higher than is indicated in the enclosed profiles. The film thickness on a slide is calculated from a calibrated sputter rate and the amount of time it takes to remove the film. It is assumed that the deposited film has been removed when the percentage of contaminants in the sputtered material drops below half of the original atomic concentration. In this study, the carbon concentration profile was used. To determine a sputter rate for this procedure, sample #19 was sputtered at a region that was partially masked with aluminum foil. A surface profile was then determined across this interface. This profilometer scan shows that approximately

8400 Å was removed in 60 minutes of sputtering to give a sputter rate of approximately 140 Å/min. The measurements showed that the initial composition of the control plates consisted of carbon. Surface adsorption of hydrocarbons is common for many materials. The concentrations of carbon on the control samples were significantly lower. The AES measurements showed that the carbon film was quickly removed during surface sputtering, therefore it was only a surface feature.

Samples #3 and #4 were difficult to investigate. The profile between 40 and 90 minutes of sputtering sample #3 was lost because surface charging caused the Auger peaks to shift outside the pre-selected energy window. This method was not designed for extremely large depths because sputtered material begins to redeposit on the plates and significantly affects the results. As a result interpreting the profile for #3 was not possible. For sample #4 the concentrations in the AES profile changed very gradually. This result may be due to the fact that the substrate beneath the film was etched somewhat during deposition of the film. In most cases, the interface between the fluorocarbon film and the quartz plate is relatively sharp. A typical AES profile is shown in Figure 6 and the AES film thickness are shown in Table 1.

Both the mass/loss and deposition/ablation measurements were required to explain the results of the experiment. Plates #12-16 in the symmetric plane should mirror measurements made on plates #21-17, respectively, if the plume was symmetric. There was significant ablation and mass loss on the plates within 30° on either side of the thruster centerline. There was mass gain and film deposited on the remaining quartz samples in that plane. However, the quantity of mass/loss gain or thickness loss/gain on opposing plates do not correlate with each other. For instance, samples #15 and #18 should be mirror images of each other; they had similar changes in thicknesses but the mass loss of #15 was greater than the mass loss of #18 by a factor of two. While plates #16 and #17 experienced similar mass loss, the ablation depth of #16 was almost three times greater than the ablation depth of #17. The differences in ablation depth might be explained by slight misalignments in the collimators, since those measurements are taken near the sample edges, and all four corners of a slide were not checked for uniform thickness changes. However, the mass loss is a global measurement and can not be accounted for in that manner. Similarly, opposing plates in the deposition region, do not necessarily experience a similar mass gain and deposition thickness though the differences are much less dramatic.

The deposition/mass loss profile is more complex in the asymmetric plane. In the asymmetric plane, plates #5 through #7 showed both mass loss and ablation on the

plates. Plate #6 is parallel to the centerline of the thruster. There was no opposing sample. Plates #5 and #7 are located 10° on either side of #6. Plate #5 showed 75% less mass loss but twice ablation depth of #7. Plates #4 and #8 are the most different. Plate #4 had both mass gain and deposition on the surface, while #8 showed significant mass and thickness loss. Similarly with opposing pair #3 and #9, #3 showed mass gain, while #9 showed no mass change but some deposition. The remaining opposing pairs #1 and #11, and #2 and #10 showed both mass gain and deposition, though the results are not nearly as dramatic as the plates that were in the direct plume path. As was anticipated from the previous study, where the plume was attracted to the cathode electrode resulting in an off-axis thrust component, plate #8, which is on the cathode side of the array, showed greater plume impacts. It is particularly clear that the net effect of the direct plume is ablation; how much deposition also takes place is not easily quantified. This result leads to the conclusion that the PPT plume produces a complex deposition and ablation process on exposed surfaces.

The spectrometer was used to measure the reflectance and transmittance of each of the samples. The integrated reflectance and transmittance is given in Table 1, and samples of the actual reflectance and transmittance curves versus the wavelength are shown in Figures 7 through 14. Pre-test transmittance measurements were made on all the quartz plates, and they were nearly identical. The pre-contamination curve shown in Figure 7 is representative of pre-contamination transmittance profiles for all the samples. The small disturbance at 860 nm seen in the plots of reflectance and transmittance is due to a lamp change within the spectrometer itself. The figure also shows the post-contamination transmittance measurements for samples #1 through 6. Figures 8 through 10 show only the post-test data where each figure contains data from one quadrant of an array. In all of the figures, contamination seems to have the largest impact on wavelengths below 550nm. Figure 7 shows the most significant change in transmittance in that wavelength range. The transmittance measurements shown in that graph were taken on samples collected in the asymmetric array in the quadrant away from the plume flow. In that quadrant, samples #3 and 5 experienced more deposition and less of the ablative effects of the direct plume. The other three figures show results that seem to follow the same general trends.

Similarly, in Figure 11 there is a single curve that was representative of a pre-contamination reflectance

profiles for all the samples. In this instance, these data are for sample #1 and the post-test data for samples #1 through 6 are also included. Figures 12 through 14 show only the post-test contamination data where each figure contains data from one quadrant of an array. In all the figures, contamination seems to have less impact on the reflectance than on the transmittance, as evidenced by higher resolution of the y-axis in the figures. Figure 11 showing data from the first quadrant in the asymmetric array has the largest changes. When comparing the samples in Figure 11 with those in Figure 12, the asymmetry of the plume is obvious. Samples #1 and 2 and samples #11 and #10, which are well outside the plume, have very similar reflectance trends over the wavelength range. Samples #5 and 7, which are well with main body of the PPT plume, also have similar trends. However, samples #3 and 4 have very different trends samples from the coinciding samples #9 and 8 on the other quadrant of the array. Figures 13 and 14 have very similar trends for opposing samples on either side of the symmetric array and a more tightly grouped series of curves. Like the asymmetric array, the biggest differences are in the opposing samples located in the plume fringes, but to a much less degree.

The composition of the films as determined by the AES measurements, which are shown in Table 1, indicate various combinations of Cl, C, N, O, F, Fe, Si and Ni. The carbon and fluorine are expected constituents of the ablated propellant. The Ni, Fe, Cl, N, O and C are constituents found in the PPT components, mainly the electrode pairs, spark plug, and surrounding materials. The Si and O are the constituents of quartz.

Experimental results applied to instrument visibility for ST-3
The results from the analysis of the films collected on the witness plates in the PPT plume were used to determine the effect of these films on $\Gamma_{Intensity}$. Additional experiments are required to determine the remaining visibility terms. The transmittance, T, and reflectance, R, measurements were used to determine the film absorptance and absorption coefficients, β, of the films with the following relationship, where z is the film thickness,

$$\frac{T}{100 - R} = \exp(-\beta z).$$

The properties of the films deposited on the witness plates throughout the plume vary significantly. As described earlier, the witness plates positioned near the axis of the thruster were etched during high energy ion bombardment. The effect of the films and surface structure cannot be deconvolved from the measurements taken. Therefore, the films applied to determine instrument visibility were taken at large angles off the thruster axis which were not under direct bombardment from high energy ions: samples 12, 13, 20, and 21. These

collected films should also be the most similar to the films deposited on a spacecraft surface not located in the direct line of sight of the thruster, which will most likely be the case for the instruments on-board. The samples considered were positioned in the symmetric plane of the thruster. Figure 15 shows the calculated β for samples 12, 13, 20, and 21.

The absorption coefficient can be modeled in the spectral range of interest and then applied to studies considering film thicknesses, z (nm), anticipated on spacecraft surfaces and then their effect on $\Gamma_{Instrument}$. The curve fit through the four β curves is shown in Figure 15 and defined by

$$\beta = -8.7233x10^{-6} + 0.13816\exp(-0.01559\lambda),$$

where λ (nm) is the wavelength. The transmittance of the films is then represented by

$$T = \exp(-\beta z),$$

when the reflectance of the films is negligible. The absorption coefficient β is related to the imaginary component of the complex index of refraction, n_I, by $\beta = 2n_I/\lambda$.

The $\Gamma_{Intensity}$ can then be calculated from the two known cumulative film thicknesses which each of the two signals will pass through before reaching the combiner. Blandino et al.[8] estimated that a film thickness of 6 nm could be expected during 5 months of operation for a system delivering 1.4 mN at 2.0 Hz for one potential spacecraft configuration. The source-target separation varied from 100m to 1000m over this period so the deposition would be expected to be much less than the laboratory case with the witness plate in close proximity to the PPT (flux decreasing as the inverse square of the separation). Across the range of wavelengths investigated, the films obtained in the experiments discussed in this article increased the reflectance of the quartz witness plates by less than 0.8% for films less than 710 nm thick, and decreased the reflectance of the films by no more than 3 % for 200 and 340 nm thick films. For a 6 nm film, the effect on the reflectance of the surfaces will be negligible. The decrease in transmittance will be most significant at the lowest wavelength, 350 nm. With a 6 nm film thickness and 350 nm wavelength, the transmittance of the film will be 99.64%. The transmittance will increase with increasing wavelength until it reaches 100% at 620 nm.

A worst case scenario for visibility loss through intensity can be evaluated by assuming that only the collector spacecraft collects a 6 nm film. The source signal will pass through a total 24 nm of film after reflecting off of both sides of the siderostat and transfer flat. This film thickness corresponds to a transmittance of 98.61% at a wavelength of 350 nm, K=0.9861, and a $\Gamma_{Intensity}$ of 0.999975, assuming the second signal is transmitted at 100%. A 340 nm film would reduce the signal transmittance to 45.38% and $\Gamma_{Intensity}$ to 0.9267, assuming that the intensity of one signal is 45.38% of the second signal. At this film thickness, the reflectance should still be negligible, but the visibility loss through intensity is not negligible. Nevertheless these calculations suggest, the effect of the thruster effluents should be negligible on the instrument visibility for the missions in which the expected film thickness is 6 nm or less. These calculations should be refined when the spacecraft and propulsion system configurations for specific missions are known.

Conclusions

Analysis of the fluorocarbon films deposited by the breadboard PPT showed that the film deposition profile in the plume was qualitatively consistent with off-axis thrust measurements previously acquired. The results showed that the plume was canted towards the cathode electrode. An asymmetric deposition and ablation pattern was observed in the asymmetric thruster plane. A net ablation and surface roughening was observed on the witness plates positioned within 10° of the thruster axis because of the high density of high energy ions in this region. Net film deposition was observed on witness plates positioned 50° from the thruster axis and at larger angles on the cathode side of the asymmetric plane. Net film deposition was observed on witness plates positioned at an angle as low as 30° on the anode side of the asymmetric plane. In the symmetric plane, net deposition was observed on plates positioned at angles greater than 30° from the thruster axis, while net ablation occurred within this half-cone angle.

Results from the investigation of the transmittance losses through fluorocarbon films expected on spaceborne interferometer systems with PPTs showed a negligible impact on instrument visibility. These calculations were based on the film absorptance coefficient calculated from the reflectance and transmittance measurements. These calculations should be further refined when film deposition rates on the siderostat and transfer flats are known for specific missions and spacecraft configurations.

Determining the total impact of the films of thruster effluents on $\Gamma_{Instrument}$ will be the subject of future studies. RMS films thickness must be measured to evaluate the wavefront distortions induced by the films and $\Gamma_{Wavefront}$. The dimensions and size distributions of particulates in the films of thruster effluents must be quantified to determine Γ_{Area} and $\Gamma_{Wavefront}$. The index of refraction of

the films must be measured to determine the frequency dependant phase shift induced by the films and $\Gamma_{Dispersion}$.

<div style="text-align:center">References</div>

1. Burton, R.L., and Turchi, P.J. "Pulsed Plasma Thruster", Journal of Propulsion and Power, Volume 14, Number 5, pp. 716–735.

2. Brill, Y., Eisner, A., and Osborn, L., "The Flight Application of a Pulsed Plasma Microthruster; The NOVA Satellite", AAIA paper 82–1956, Nov. 1982.

3. Maag, C.R., and Millard, J.M., "Results of NOVA-3 Contamination Monitoring Equipment", AFAL–TR–87–107, Dec. 1987.

4. Arrington, L.A., and Haag, T.W., "Multi-Axis Thrust Measurements of the EO-1 Pulsed Plasma Thruster", AIAA–99–2290, June 1999.

5. Arrington, L.A., Haag, T.W., Pencil, E.J., and Meckel, N.J., "A Performance Comparison of Pulsed Plasma Thruster Electrode Configurations", IEPC 97–127, August 1997.

6. Myers, R.M., Arrington, L.A., Pencil, E.J., Carter, J., Heminger, J., Gatsonis, N., "Pulsed Plasma Thruster Contamination", AIAA 96–2729, July 1996.

7. Spanjers, G.G., Lotspeich, J.S., McFall, K.A., and Spores, R.A., "Propellant Inefficiency due to Particulates in a Pulse Plasma Thruster", STAIF-97, January 26–30, 1997, pp. 323–328.

8. Blandino, J.J., Cassady, R.J., Peterson, T.T., "Pulsed Plasma Thruster for the New Millenium Interferometer (DS-3) Mission," IEPC 97–192, August 1997.

9. Lay, O., Blackwood, G., Cornford, S., Dubovitsky, S., Gorham, P., Linfield, R., "ST-3 Instrument Requirements and Design Document,"JPL document.

Table 1: Post-Test Contamination Data For Asymmetric, Symmetric and Control Samples.

Sample #	Angular Location, Degrees	Mass (Loss)/Gain mg[1]	Post-Test % Transmittance	Post-Test % Reflectance	AES Surface scan	Deposition Thickness (Loss)/Gain, Å
1	0	0.09	88.9	9.6	Cl,C,N,O,F,Fe,Ni	1680
2	20	0.23	87.7	6.8	C,N,F	4200
3	40	0.71	75.5	8.5	C,O,Fe,F[2]	NA
4	60	1.05	64.6	11.8	C,O,Fe,F[2]	8000[1]
5	80	(13.62)	64.4	8.2	---	(93000)[1]
6	90	(18.24)	44.0	6.2	---	(83000)[1]
7	100	(18.12)	66.7	7.4	---	(47000)[1]
8	120	(5.05)	87.3	5.1	C,O,F[2]	(49000)[1]
9	140	(0.02)	80.8	8.7	Cl,C,N,O,F,Fe,Ni	2900
10	160	0.11	86.8	7.0	Cl,C,N,O,F,Fe,Ni	4900
11	180	0.06	88.4	9.3	Cl,C,N,O,F,Fe,Ni	840
12	0	0.06	92.5	6.3	C,N,F	3400
13	20	0.25	90.8	6.5	C,F	5500
14	40	0.07	88.7	6.3	C,N,O,F	6000
15	60	(7.33)	81.7	5.9	C,O[3]	(34000)[1]
16	80	(19.38)	64.7	7.5	---	(167000)[1]
17	100	(18.07)	68.4	8.0	---	(60000)[1]
18	120	(3.77)	79.7	6.9	---	(31000)[1]
19	140	0.33	87.4	6.5	C,N,F	12000
20	160	0.25	91.2	6.8	C,N,F	7100
21	180	0.09	93.1	6.2	C,N,F	2000
22	Control	0.00	93.3	6.9	Si,C,N,O	
23	Control	0.02	93.2	7.1	Si,C,O	
24	Control	(0.05)	93.3	7.0	Si,C,O	

[1]profilometer measurement
[2]surface charging

Asymetric View

PPT

[A | C]

0° #1

61cm

Direction of Plume

20° #2

#3
40°

#4
60°

#5
80°

#6

C̷L
90°

#7
100°

#8
120°

#9 140°

#10 160°

20°

#11 180°

Symmetric View

PPT

0° #12

Direction of Plume

#13
20°
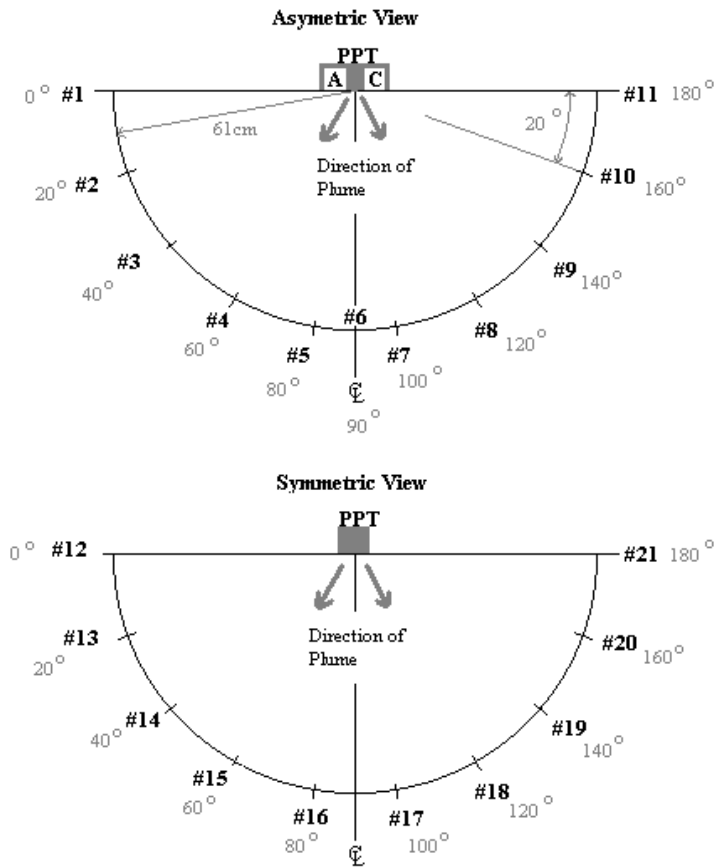
#14
40°

#15
60°

#16
80°

C̷L

#17
100°

#18 120°

#19 140°

#20 160°

#21 180°

Figure 1: Collimator/Sample Locations Relative to the PPT Where
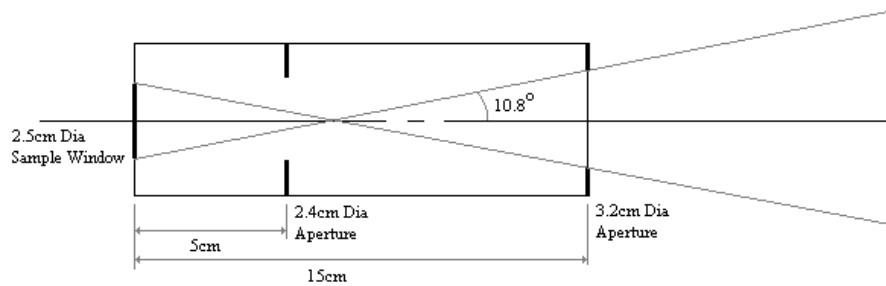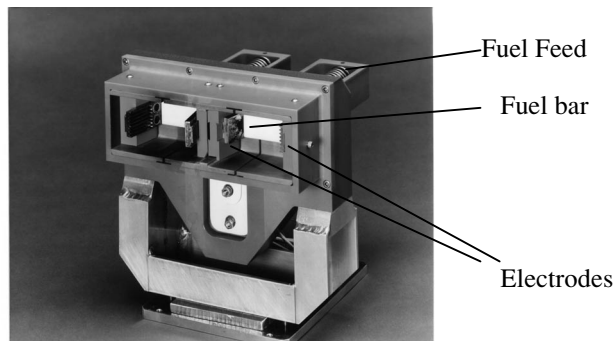A = Anode Electrode and C = Cathode Electrode.

2.5cm Dia
Sample Window

10.8°

2.4cm Dia
Aperture

3.2cm Dia
Aperture

5cm

15cm

Figure 2: Collimator.

Fuel Feed

Fuel bar

Electrodes

Figure 3: NASA/Primex Breadboard PPT.

"Contaminated Region" | Original Quartz Surface
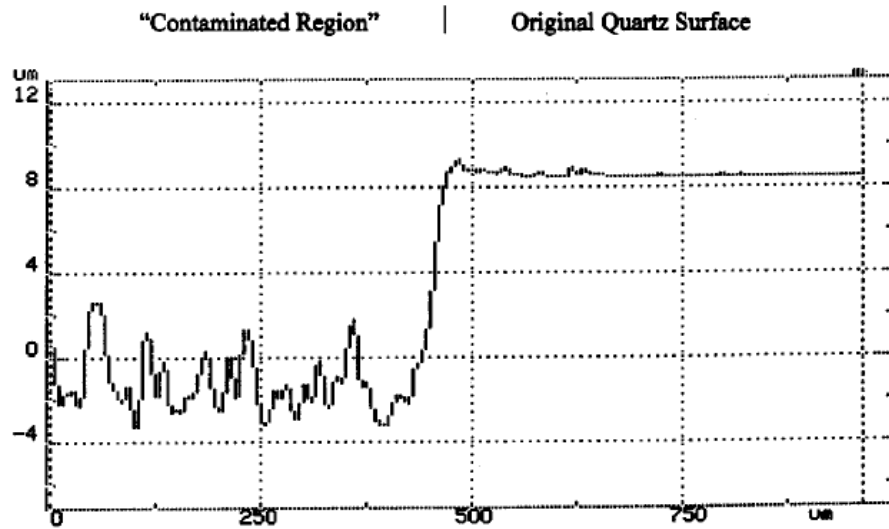
Figure 4: Profilometer Measurement for Sample #5.
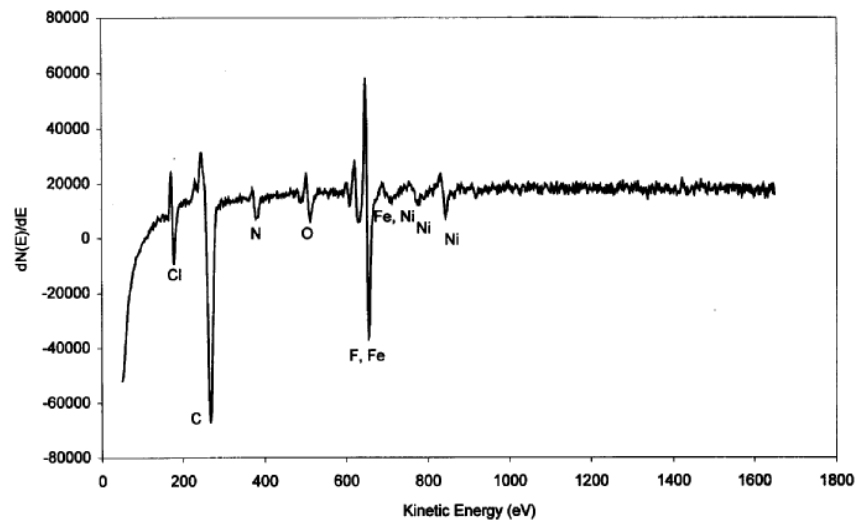
Figure 5: AES Surface Scan for Sample #10.
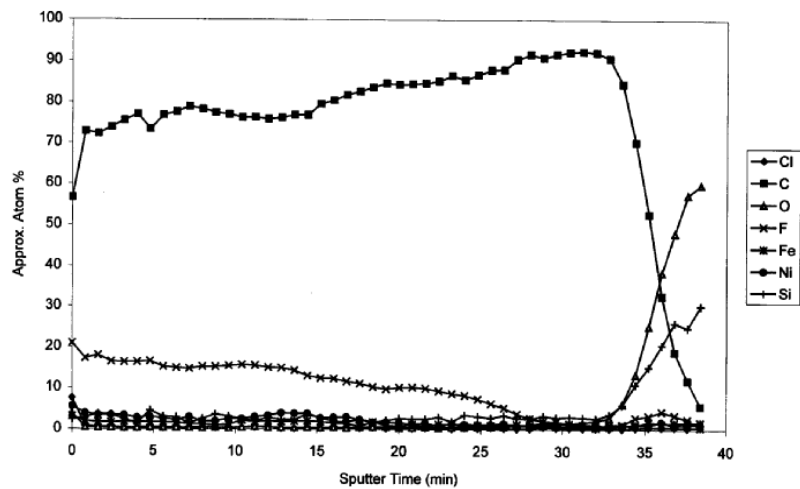
Figure 6: AES Profile for Sample #10.
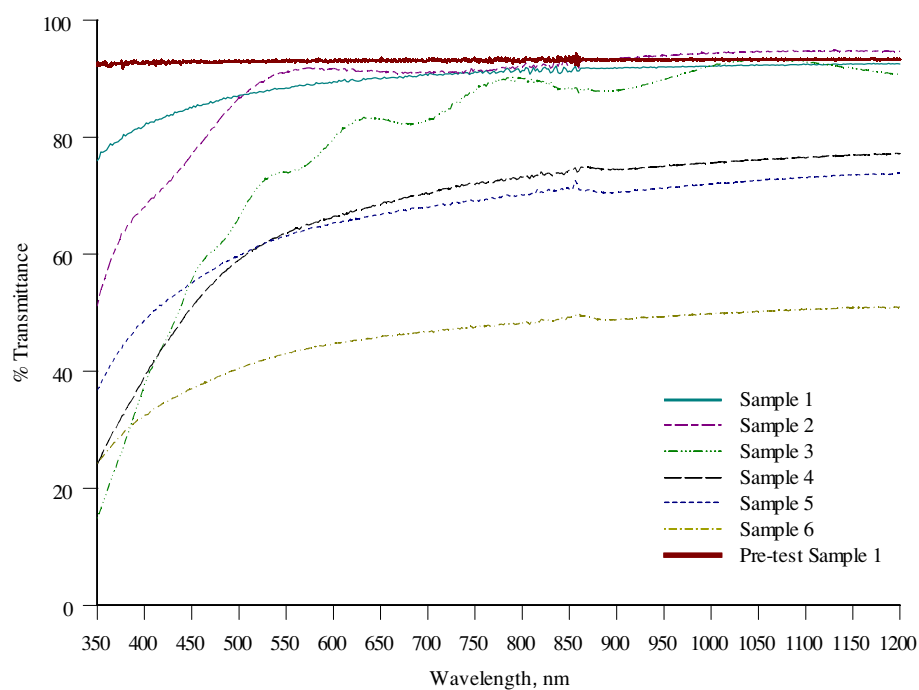
Figure 7: Post Contamination Transmittance Measurements on Asymmetric Plane
from 0 to 90° and Pre-Test Transmittance Measurement on Sample 1.
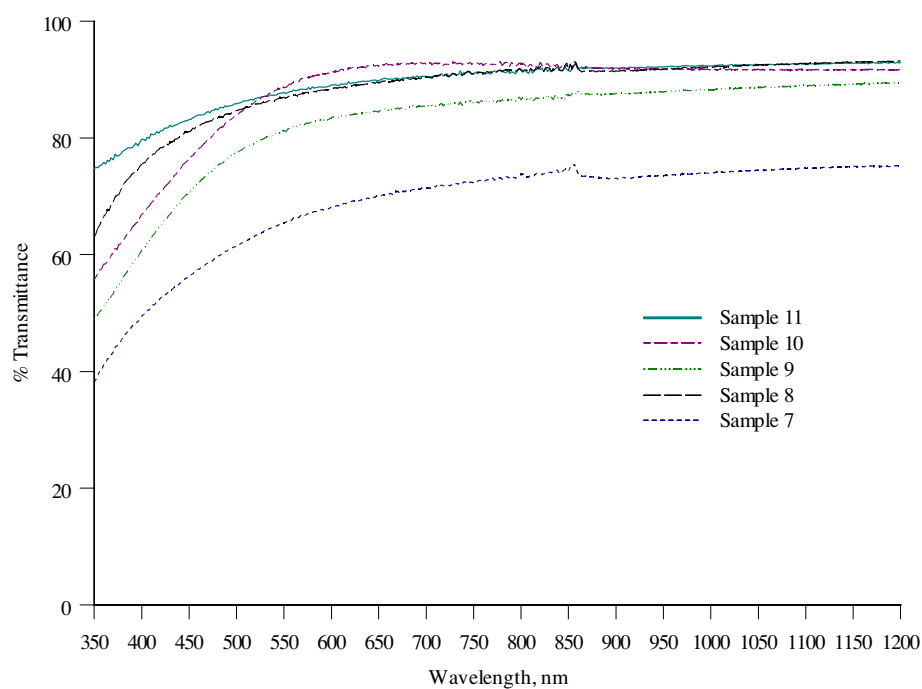
Figure 8: Post Contamination Transmittance Measurements
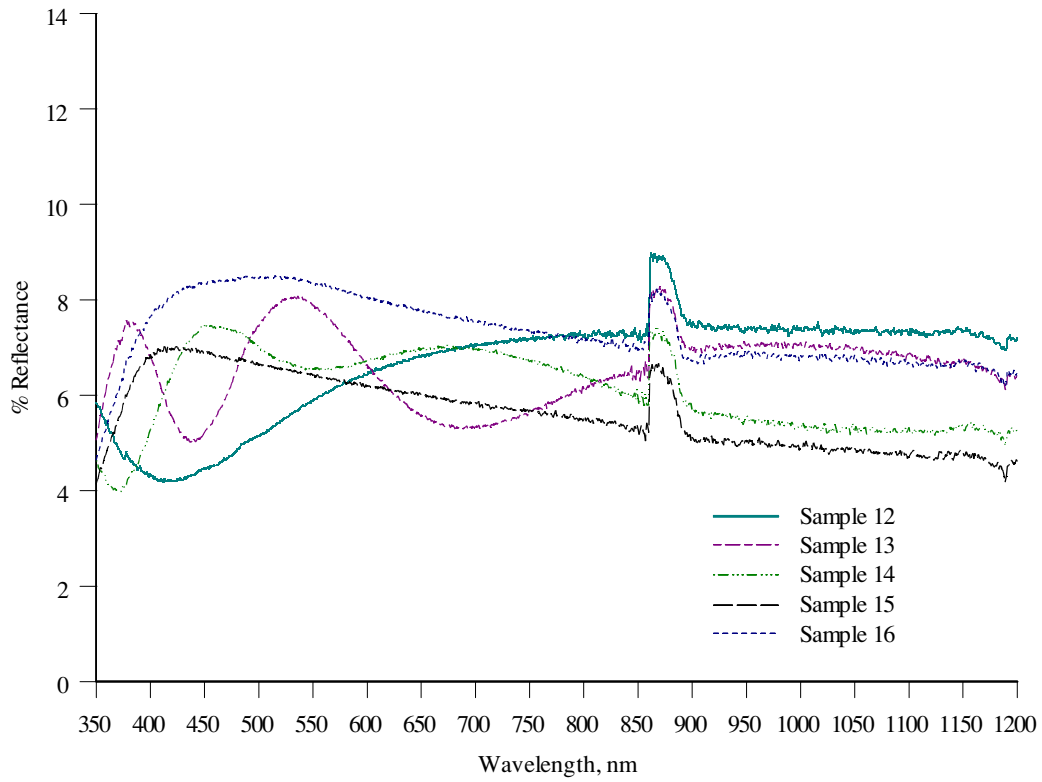on Asymmetric Plane from 100 to 180°.
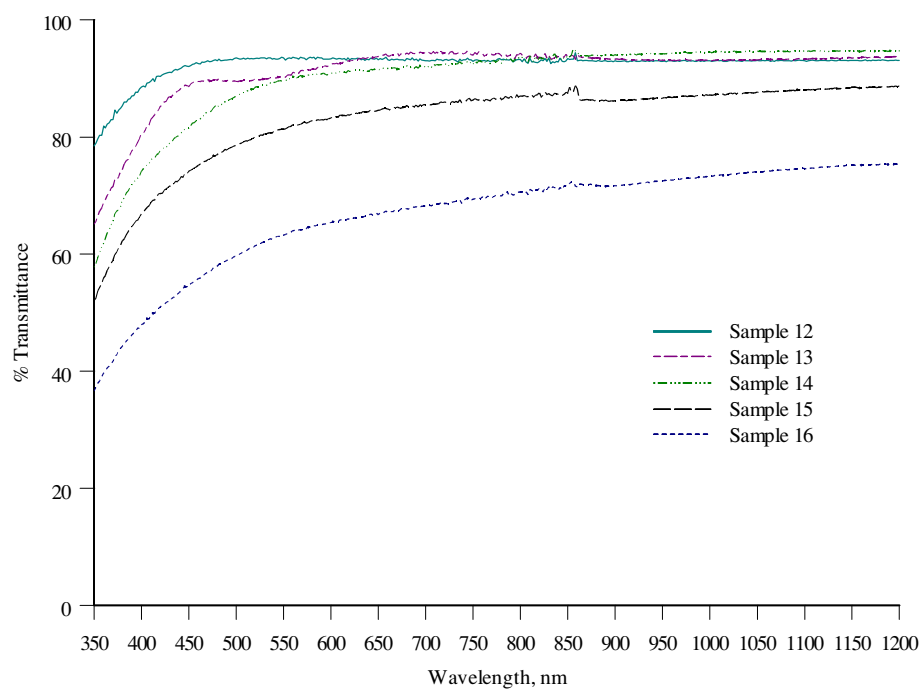
Figure 9: Post Contamination Transmittance Measurements on
Symmetric Plane from 0 to 80°.
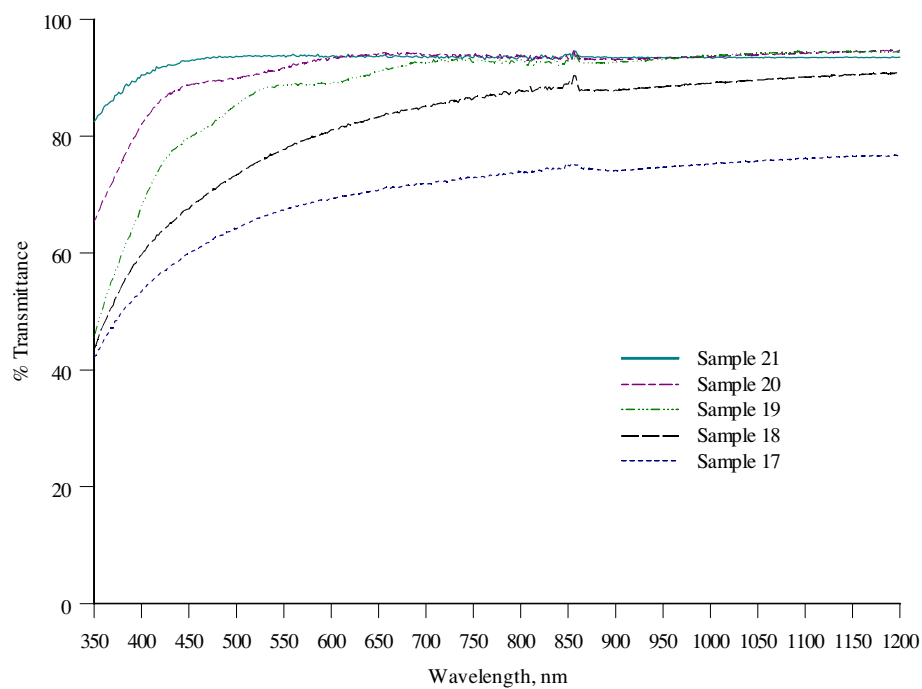
Figure 10: Post Contamination Transmittance Measurements on
Symmetric Plane from 100 to 180°.
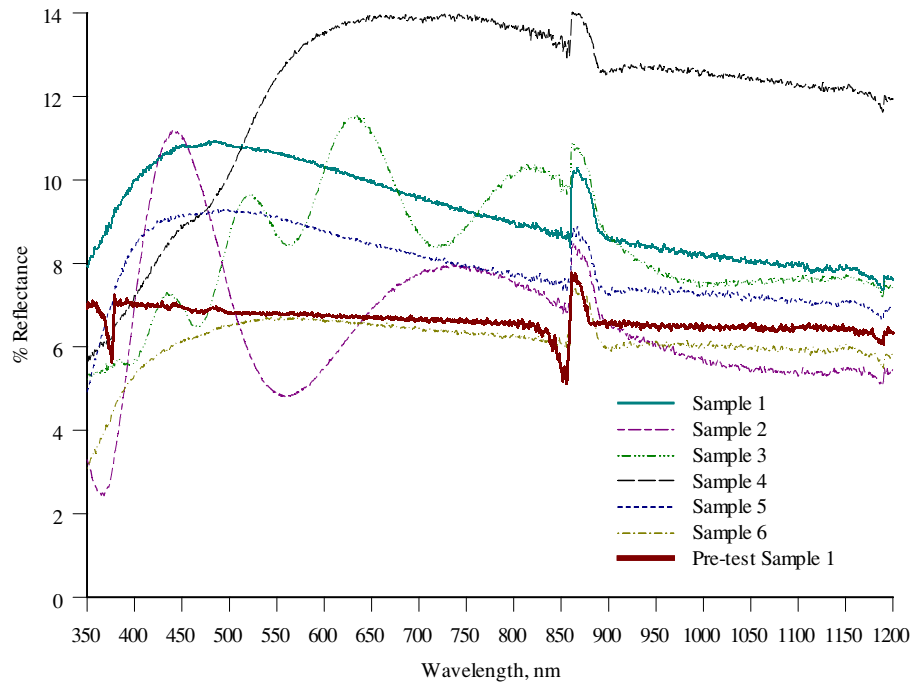
Figure 11: Post Contamination Reflectance Measurements on Asymmetric Plane from 0 to 90° and Pre-Test Reflectance Measurements of Sample 1.
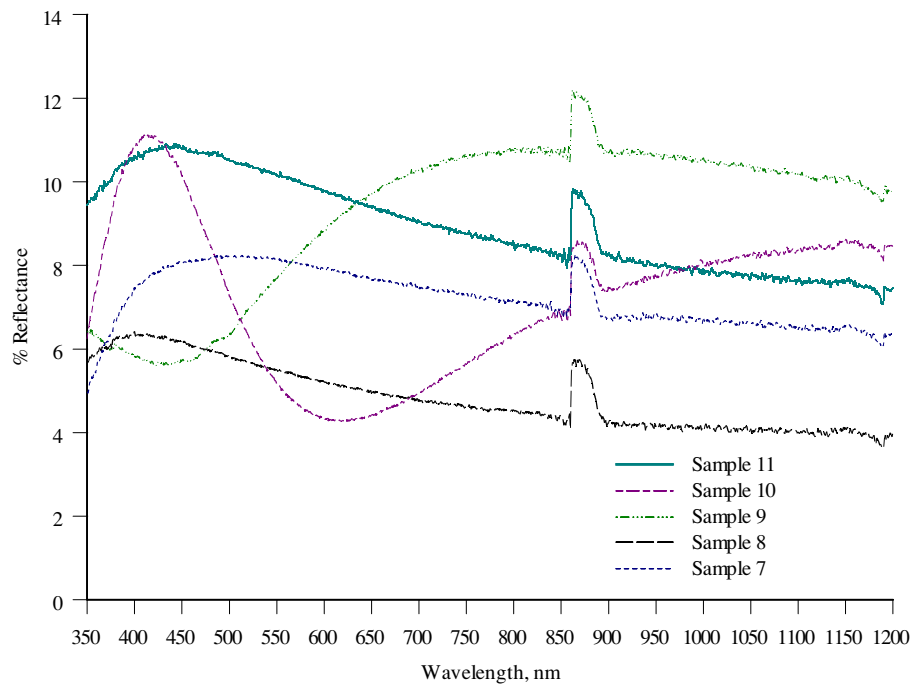
Figure 12: Post Contamination Reflectance Measurements on Asymmetric Plane from 100 to 180°.

Figure 13: Post Contamination Reflectance Measurements on Symmetric Plane from 0 to 80°.
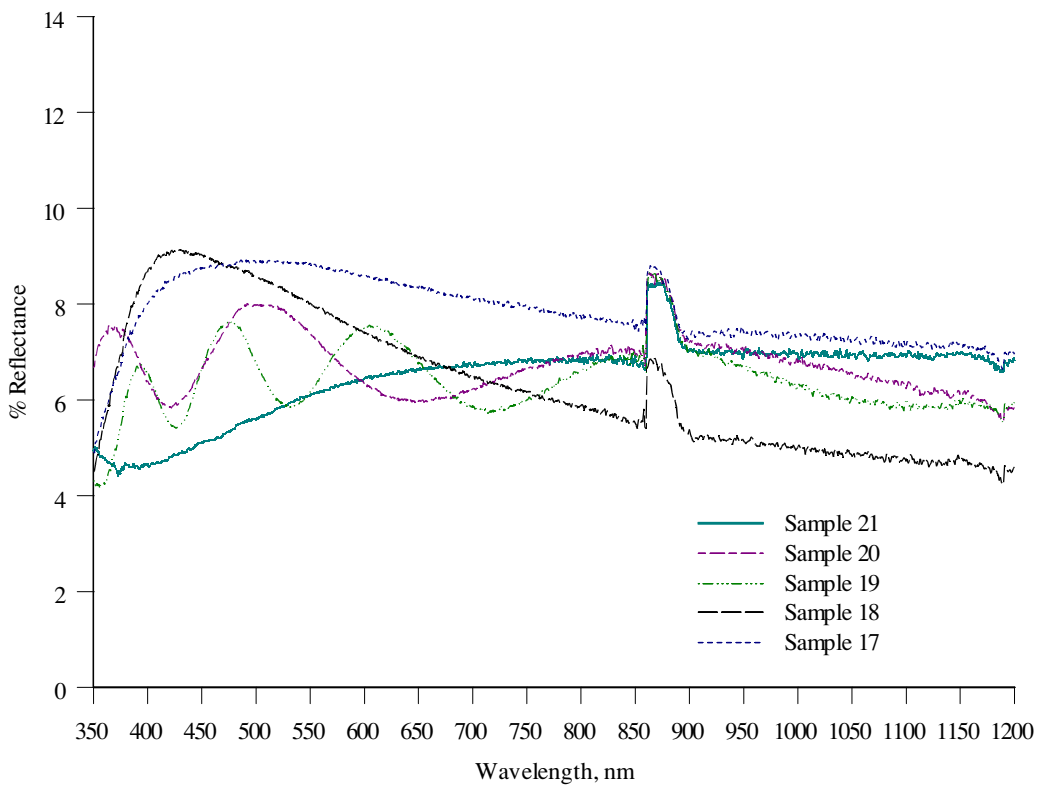
Figure 14: Post Contamination Reflectance Measurements on Symmetric Plane from 100 to180°.
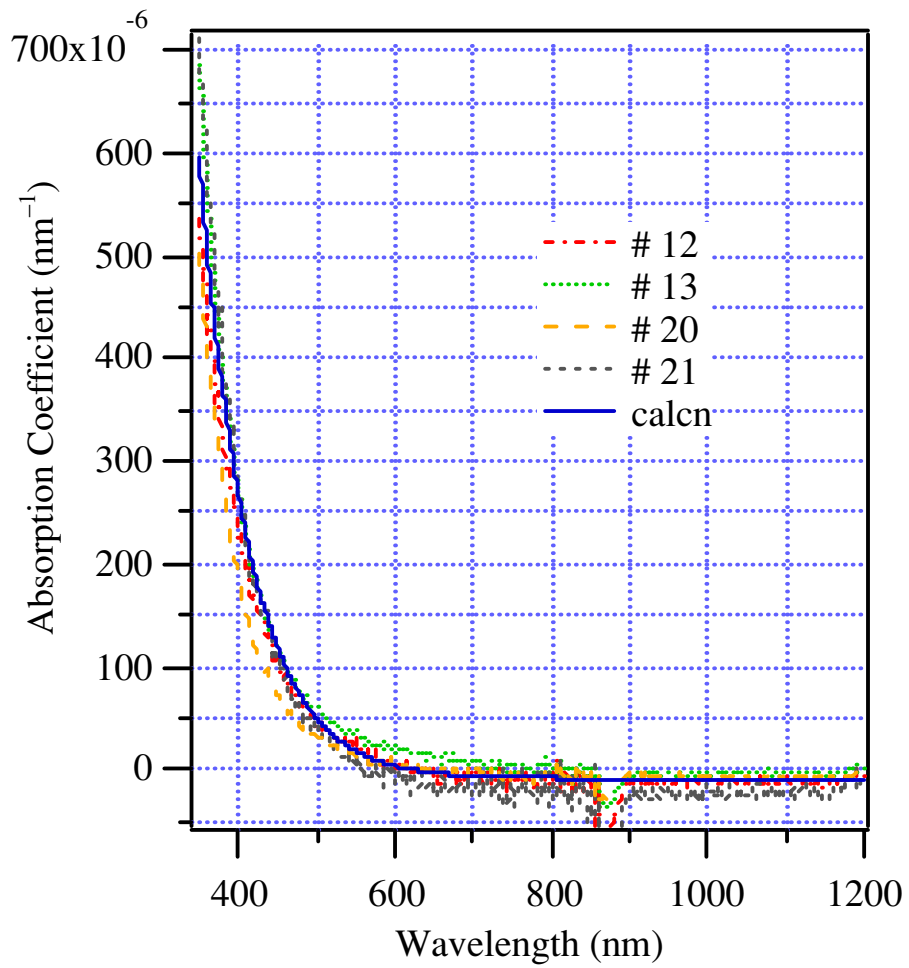
Figure 15: Absorption Coefficients for Samples 12, 13, 20, and 21.

REPORT DOCUMENTATION PAGE

1. AGENCY USE ONLY (Leave blank)	2. REPORT DATE	3. REPORT TYPE AND DATES COVERED
	September 2000	Technical Memorandum

4. TITLE AND SUBTITLE

Pulsed Plasma Thruster Plume Study: Symmetry and Impact on Spacecraft Surfaces

5. FUNDING NUMBERS

WU–632–1B–1B–00

6. AUTHOR(S)

Lynn A. Arrington, Colleen M. Marrese, and John J. Blandino

7. PERFORMING ORGANIZATION NAME(S) AND ADDRESS(ES)

National Aeronautics and Space Administration
John H. Glenn Research Center at Lewis Field
Cleveland, Ohio 44135–3191

8. PERFORMING ORGANIZATION REPORT NUMBER

E–12412

9. SPONSORING/MONITORING AGENCY NAME(S) AND ADDRESS(ES)

National Aeronautics and Space Administration
Washington, DC 20546–0001

10. SPONSORING/MONITORING AGENCY REPORT NUMBER

NASA TM—2000-210364
AIAA–2000-3262

12a. DISTRIBUTION/AVAILABILITY STATEMENT

Unclassified - Unlimited
Subject Category: 20   Distribution: Nonstandard

This publication is available from the NASA Center for AeroSpace Information, (301) 621–0390.

12b. DISTRIBUTION CODE

13. ABSTRACT (Maximum 200 words)

Twenty-four witness plates were positioned on perpendicular arrays near a breadboard Pulsed Plasma Thruster (PPT) to collect plume constituents for analysis. Over one million shots were fired during the experiment at 43 J using fluorocarbon polymer propellant. The asymmetry of the film deposition on the witness plates was investigated with mass and thickness measurements and correlated with off-axis thrust vector measurements. The composition of the films was determined. The transmittance and reflectance of the films were measured and the absorption coefficients were calculated in the wavelength range from 350 to 1200 nm. These data were applied to calculate the loss in signal intensity through the films, which will impact the visibility of spaceborne interferometer systems positioned by these thrusters.

14. SUBJECT TERMS

Pulsed plasma thruster; Contamination; Off-axis; Reflectance; Transmittance; Visibility coefficients

15. NUMBER OF PAGES

21

16. PRICE CODE

A03

17. SECURITY CLASSIFICATION OF REPORT	18. SECURITY CLASSIFICATION OF THIS PAGE	19. SECURITY CLASSIFICATION OF ABSTRACT	20. LIMITATION OF ABSTRACT
Unclassified	Unclassified	Unclassified	